EUROfusion

EUROFUSION WPJET1–PR(14)12

A.V. Chankin et al.

Influence of the ExB Drift in High Recycling Divertors on Target Asymmetries

Preprint of Paper to be submitted for publication in
Plasma Physics and Controlled Fusion

This work has been carried out within the framework of the EUROfusion Consortium and has received funding from the Euratom research and training programme 2014-2018 under grant agreement No 633053. The views and opinions expressed herein do not necessarily reflect those of the European Commission.

Influence of the E×B Drift in High Recycling Divertors on Target Asymmetries

A.V.Chankin[1], G.Corrigan[2], M.Groth[3], P.C.Stangeby[4] *and JET contributors**

EUROfusion Consortium, JET, Culham Science Centre, Abingdon, OX14 3DB, UK
[1]Max-Planck-Institute for Plasma Physics, Garching bei München, Germany
[2]Culham Centre for Fusion Energy, Abingdon, Oxfordshire, United Kingdom
[3]Aalto University, Otakaari 4, Espoo, Finland
[4]University of Toronto Institute for Aerospace Studies, Toronto, Canada

Abstract

Detailed analysis of convective fluxes caused by E×B drifts is carried out in a realistic JET configuration, based on a series of EDGE2D-EIRENE runs. The EDGE2D-EIRENE code includes all guiding centre drifts, E×B as well as ∇B and centrifugal drifts. Particle sources created by divergences of radial and poloidal components of the E×B drift are separately calculated for each flux tube in the divertor. It is demonstrated that in high recycling divertor conditions radial E×B drift creates particle sources in the common flux region (CFR) consistent with experimentally measured divertor and target asymmetries, with the poloidal E×B drift creating sources of an opposite sign but smaller in absolute value. That is, the experimentally observed asymmetries in the CFR are the opposite to what poloidal E×B drift by itself would cause. In the private flux region (PFR), the situation is reversed, with poloidal E×B drift being dominant. In this region poloidal E×B drift by itself contributes to experimentally observed asymmetries. Thus, in each region, the dominant component of the E×B drift acts so as to create the density (and hence, also temperature) asymmetries that are observed both in experiment and in 2D edge fluid codes. Since the total number of charged particles is much greater in the CFR than in PFR, divertor asymmetries caused by the E×B drift should be attributed primarily to particle sources in the CFR caused by radial E×B drift.

** See the Appendix of F. Romanelli et al., Proceedings of the 25th IAEA Fusion Energy Conference 2014, Saint Petersburg, Russia*

1. Introduction

Asymmetries between plasma parameters at divertor target plates can be influenced by cross-field drifts (see e.g. [1]). In this paper, we will be assuming a single null divertor configuration of tokamaks unless otherwise stated. The plasma-wall interaction is most intense at the two divertor targets, which are usually referred to as the inner (high magnetic field side) and outer (low field side) targets. The adjacent parts of the divertor are usually referred to as inner and outer divertors. Experimentally measured divertor and target asymmetries are known to be dependent on the direction of the ion grad-B drift: towards (in the 'normal' toroidal field, B_t, configuration) or away (in the 'reversed' field configuration) from the divertor (see e.g. review paper [2] and refs. therein). Since reversing the direction of the toroidal magnetic field in a tokamak changes the direction of all cross-field drifts, dedicated 'field reversal' experiments, as well as theoretical understanding and modelling of the drift affects in the scrape-off layer (SOL) and divertor have been an important part of plasma edge physics research.

Early models aimed at explaining the influence of the E×B drift on target asymmetries invoked *poloidal* E×B drift. In the SOL, positive radial electric field ($E_r = -\partial\Phi/\partial r$) in the plasma is expected. This is related to the electron temperature (T_e) radial decay from the last closed flux surface (LCFS, coinciding with the magnetic separatrix in divertor configurations) to the wall and the presence of the Debye and Chodura sheath (with the latter often referred to as the magnetic pre-sheath) drop between the plasma and the target ($\sim 3T_e/e$, see e.g. [1]). Simple models [3-5] assumed equal and poloidally constant electron and ion temperatures, the absence of neutral recycling and ionization sources at the targets, and a simple cylindrical configuration, without toroidal effects. Particle conservation and poloidal momentum balance equations included cross-field terms attributed to poloidal velocity $V_E = cE_r / B$, and the Bohm boundary condition for the ion parallel velocity at the targets was modified: poloidal projection of the total poloidal velocity $V_\theta = V_{i,\|} B_\theta / B + V_E$ was equated to the poloidal projection of the ion sound speed $c_s B_\theta / B$. The models yielded expressions for the target pressure asymmetry (equal to the density asymmetry owing to the $T_{e,i}(\theta) = const$ assumption)

$$\frac{p_{out}}{p_{in}} = \frac{2 + M_E}{2 - M_E}, \qquad (1)$$

where $M_E = \frac{cE_r}{B_\theta c_s}$ and $c_s = \sqrt{(T_e + T_i)/m_i}$, see e.g. Eq. (18.40) of Ref. [1]. The pressure is larger at the target towards which the poloidal drift velocity V_E is directed. One expects that, if these simple models were extended to include neutral recycling and divertor impurity radiation effects, together with energy conservation assumptions (rather than the $T_{e,i} = const$ assumption) that this would result in opposite trends for electron density, n_e, and temperature, $T_{e,i}$, asymmetries. Namely, in the normal B_t configuration one would expect denser and cooler plasma at the outer target, with the opposite asymmetries in the reversed B_t configuration.

As more experimental evidence on divertor and target asymmetries was collected, it became clear that the above simple models contradicted experimental trends. Indeed, in the experiment switching the magnetic configuration from normal to reversed B_t led to a shift in target densities maxima from the inner to outer divertor, and opposite trends – for electron temperature (see e.g. [2] and more recent papers on UEDGE modeling of DIII-D experiments [6] and SOLPS modeling of ASDEX Upgrade experiments [7]). Density shifts were accompanied by similar shifts in target recycling and divertor impurity radiation. In fact, such a contradiction with simple models and ideas based on the effect of the poloidal E×B drift had already been observed, and a tentative explanation for it via the effect of the *radial* component of the E×B drift was presented, in Ref. [5].

Presently, drifts are implemented in several 2D fluid edge codes, in particular, in the three major codes that use numerical grids approximating experimental magnetic equilibria of existing divertor tokamaks: SOLPS [8,9], EDGE2D [10,11] and UEDGE [12,13] (Here the first reference describes basic features of the code, while the second – drifts implementation). Code runs with normal and reversed B_t have been carried out and results are found to be broadly in agreement with experimental trends.

Despite the successful implementation of drifts in the 2D fluid codes, the physics of the drift action remains somewhat obscure and arguments continue about which drifts are mainly responsible for observed divertor and target asymmetries. Recently, in an apparent contradiction with predictions of early models [3-5], Rozhansky *et al*. conjected that the poloidal E×B drift, instead of increasing plasma density at the material surface towards which it is directed, reduces it, while at the same time increasing plasma density at the surface away from which it is directed, and these density shifts can explain divertor and target asymmetries [14]. In this paper it is shown that such statements are unfounded, being actually in conflict with the model adopted in [14] (the model in [14] itself does not contradict the models in [3-5]). Such statements are therefore erroneous, see Appendix A. Similar statements have subsequently appeared in other publications by the same author(s) [15,16].

The main task of the present paper is to carry out a detailed investigation of how individual components of the E×B drift, poloidal and radial, influence particle balance in the inner and outer divertor legs and lead to density asymmetry, and via it, other asymmetries in plasma parameters between divertors and target plates. Some earlier experimental measurements which have been instrumental in establishing the E×B drift flow pattern are discussed below; however, the full picture can only be established in dedicated code runs and through their special analysis. Here, we present results of EDGE2D-EIRENE runs for JET with drifts for plasmas covering a wide range of experimental conditions, with electron density ranging from low to high densities resulting in various degrees of recycling in the divertor.

It has to be noted that, apart from drifts, other mechanisms can influence divertor asymmetries. For example, it is well accepted that one of the reasons for the denser and cooler plasma observed in the inner divertor in experiments is related to the larger circumference of the outer (low field) side of the torus, resulting in higher heat flux, and hence, higher $T_{e,i}$ in the outer divertor, even for spatially uniform transport coefficients (see e.g. [1] and refs. therein). Experimentally observed 'ballooning' of perpendicular anomalous transport, with larger transport coefficients on the outer side, can amplify this effect [1]. These mechanisms are independent of the B_t direction. Since the present paper deals with the drift effects, the emphasis is on the *shifts* in the asymmetries caused by the B_t reversal.

A difference in T_e between the two targets generates thermoelectric current along field lines which contributes to the target power flux asymmetry. Since this current is the effect of the target T_e asymmetry, which itself is strongly influenced by drifts, it is not considered in the present paper. As was demonstrated in recent SOLPS simulations of ASDEX Upgrade discharges, thermoelectric current is strongly reduced when drifts are switched off, with only currents activated [17].

2. Poloidal and radial E×B flows in the SOL and divertor

A schematic is shown in Fig. 1 of poloidal and radial E×B flows in the SOL and divertor for the case of the ion ∇B drift directed towards the divertor ('normal' field direction). The direction of the arrows assumes a typical situation in the SOL and divertor with T_e falling radially from the separatrix towards the wall and inside the private region, leading to the formation of a positive E_r in these regions. In the SOL the direction of the poloidal E×B flow is such that it brings more particles to the outer common flux region (CFR) of the divertor ('SOL-divertor', according to the nomenclature adopted in the EDGE2D code) and removes them from the inner SOL-divertor. The situation is reversed in the reversed B_t configuration. This E×B flow is expected to create divertor and target asymmetries which are opposite to those observed in experiment, as pointed out in the introduction.

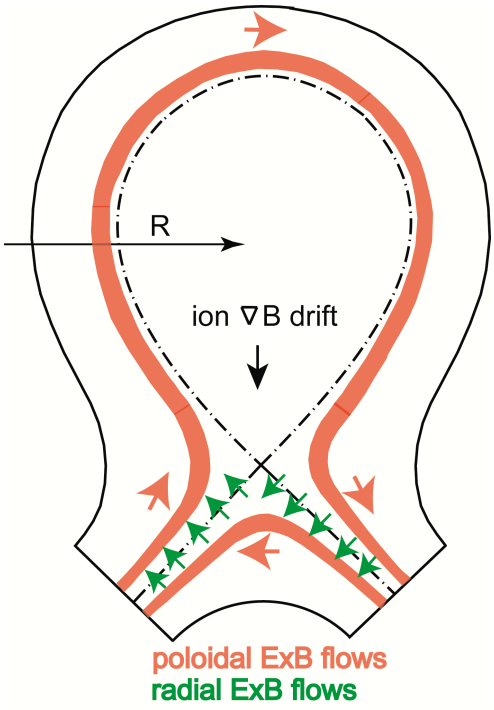

Fig. 1. Schematic of poloidal and radial E×B flows in the SOL and divertor, for the case of ion ∇B drift directed towards the divertor ('normal' field direction).

On the other hand, in the private flux region (PFR) of the divertor the direction of the poloidal E×B flow is consistent with the direction of experimentally measured divertor asymmetries. A very large value of this flow in the middle of the PFR, accounting for 25-40% of the total ion flow to the divertor targets was experimentally measured in DIII-D by a set of Langmuir probes by Boedo *et al.* [18]. Results of EDGE2D-EIRENE modeling, presented below, confirm the importance of this flow in the overall flow pattern in the divertor.

Earlier, Stangeby and Chankin [5] proposed an explanation for target asymmetries in the CFR based on radial E×B drift, by providing an estimate of the total particle flow across the separatrix in high recycling conditions (where in the parallel direction T_e drops strongly towards the target, while n_e correspondingly rises) which showed that this flow is larger than the poloidal E×B flow in the main SOL region. In this reference, however, the large poloidal E×B flow in the PFR pointed out by Boedo *et al.* [18], was not incorporated in the overall E×B flow pattern in the divertor and SOL. It was later conjected in [19] that results [18] may provide a missing link in the E×B flow pattern of [5], and that a global circulation of the E×B flow encompassing the SOL and divertor may occur. This circulation however is not expected to be complete, that is, it is likely not divergence free. Further, the full flow pattern

has to include perpendicular turbulent transport, which can be influenced by profile changes caused by E×B fluxes, parallel flows, volume particle sources (ionization and recombination) and fluxes to the targets. A schematic of the E×B drifts part of this global circulation pattern is shown in Fig. 1. In the following section, we will demonstrate, using the EDGE2D-EIRENE code output, that such an E×B drift flow circulation indeed takes place.

A shorter circuit of the E×B flow, around the X-point, was deduced from electric potential measurements in DIII-D experiments and later modeled with the UEDGE code. It was related to the existence of a potential hill at the X-point position [20]. In the EDGE2D-EIRENE code output described in this paper, however, a local maximum of the potential at the X-point location was not seen, and the potential fell only from the X-point to the targets, but not from the X-point towards the main SOL. Also, as follows from the EDGE2D-EIRENE modeling, the E×B flow pattern is not even approximately divergence free, as evidenced by relatively small poloidal E×B flows at the entrances to the divertors (see next section).

3. EDGE2D-EIRENE cases and macrozone particle exchange

EDGE2D-EIRENE cases were run in a realistic JET magnetic equilibrium of one of the pulses with the plasma current 2.5 MA and toroidal field 2.5 T in the ITER like wall (ILW) environment, with strike points on vertical targets, as described in [21]. Drifts and currents were switched on, and a self-consistent model for the radial electric field in the core was used. The grid used in these cases is shown in Fig. 3. It has 12 poloidal rings in the core region, 6 rings in the PFR and 20 in the SOL. There were 20 'radial' rows in the divertor and 51 in the main SOL and core. Only pure deuterium (no impurities) cases with drifts and currents were run. Such a choice was made partly because of issues of numerical stability of EDGE2D-EIRENE runs which also affected the choice of the generated grid. At the same time, pure D cases are also easier to analyse when detailed particle balance is required, such as in the present study.

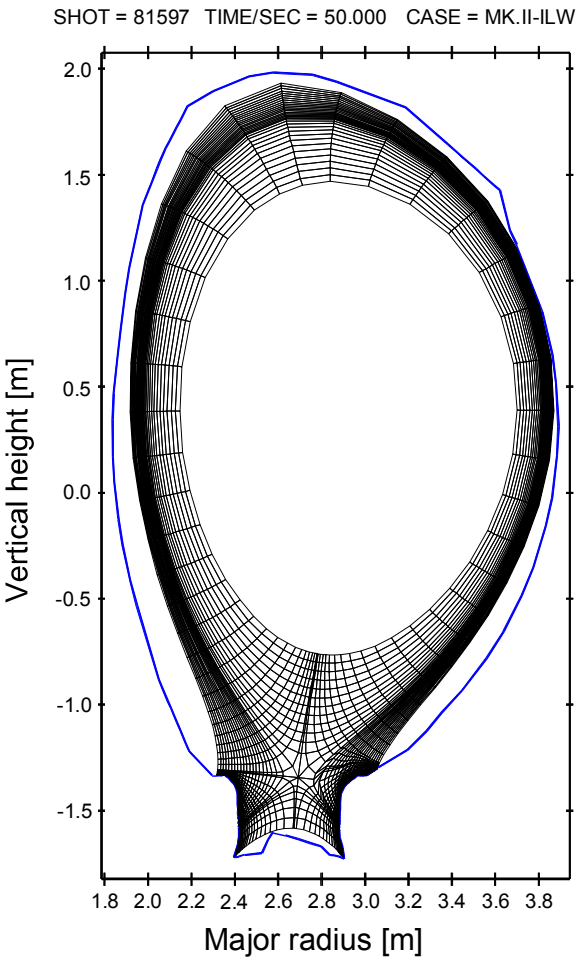

Fig. 2. EDGE2D-EIRENE grid, with 12 core (poloidal) rings, 20 SOL rings, 6 rings in the PFR, 20 'radial' rows in divertors and 51 rows in the SOL.

EIRENE version with Kotov-2008 model was used to describe neutral behaviour. Density was controlled by a combination of gas puff from the PFR and wall recycling ('puff + recycling' option in EDGE2D-EIRENE), aiming at maintaining a specified electron density at the outer midplane (OMP) position of the separatrix. Such a density control

provided equal separatrix density in normal and reversed B_t configurations and closely similar n_e and $T_{e,i}$ profiles in the main SOL, so that such pairs of cases could be directly compared. Anomalous diffusion coefficient was set at 1 m^2s^{-1} everywhere except for a narrow layer ± 1cm wide around the separatrix (in OMP cm), separating the core and SOL, where it was reduced by half. Electron and ion anomalous heat conductivities were set at 1 m^2s^{-1} in the core and PFR and 0.5 m^2s^{-1} in the SOL. Input power into the grid, 2.2 MW (corresponding to JET L-mode discharges), was equally split between ion and electron channels.

Only cases with high recycling in the divertor were run, defined as regimes where T_e falls by a factor no less than 2 from the OMP to the target(s). The lowest density cases had OMP separatrix electron density $n_s=0.7\times10^{19}m^{-3}$. The highest density cases were with $n_s=1.4\times10^{19}m^{-3}$, with this limit being set by stability of the code runs. Also, intermediate density cases with $n_s=0.9$ and 1.0×10^{19} m^{-3} were analysed. The cases were chosen so as to cover a wide range of target T_e profiles. Normal and reversed B_t cases with $n_s=0.7\times10^{19}m^{-3}$ are referred to as 'low density' due to a rather modest T_e drop from upstream to the outer target. The $n_s=0.9\times10^{19}m^{-3}$ cases are referred to as 'medium' density, due to a much more significant T_e drops. However, T_e profiles at the outer target still show maxima at positions of high ion target flux, except for the normal B_t case at the inner target, where the target T_e is always very low. The $n_s=1.0\times10^{19}m^{-3}$ cases are referred to as 'high density', since target T_e profiles have maxima outside of the area of large ion fluxes to the targets. Finally, the $n_s=1.4\times10^{19}m^{-3}$ cases are referred to as 'very high density' due to almost complete target T_e collapse in the area of high ion fluxes to the target.

After a successful run EDGE2D-EIRENE produces total particle drift flows at 'macrozone' boundaries, where all drifts (E×B, ∇B and centrifugal drifts, where the sum of the latter two for simplicity is referred to as '∇B drifts' below) are combined. The macrozones are shown in a schematic way in Fig. 3. Interfaces 1 to 5 separate inner main SOL, CFR, inner PFR, outer PFR and outer CFR regions. Interfaces 2 and 4 coincide with separatrix 'legs'. In Fig. 3, flows are given for the normal B_t case with $n_s=0.9\times10^{19}m^{-3}$. Drift flows through interfaces 1, 3 and 5 include poloidal E×B flows as the largest component while for flows through interfaces 2 and 4 it is radial E×B flows. The numbers in Fig. 3 and Table 1 are for the full toroidal circumference.

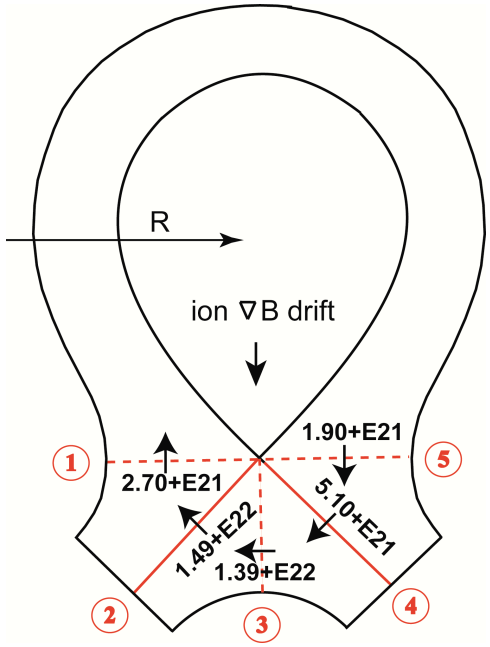

Fig. 3. Numbering of macro-zones and interfaces and drift ion flows through interfaces for a normal B_t case with $n_s=0.9\times10^{19}m^{-3}$.

As one can see from this figure, poloidal drift flows through interfaces 1 and 5 are factors 5 to 10 smaller than the flows through other interfaces. This is a typical situation for the EDGE2D-EIRENE cases analysed in these studies. The large flow through the interface 2, which is larger than the flow through the interface 3, is not typical and is a special feature of this particular case. The particle

volume sink in the inner divertor PFR caused by the difference between drift flows though interfaces 2 and 3 is confirmed by calculations accounting for only E×B flows (see below).

Flows through the interfaces for all analyzed cases are collected in Table 1. The sign convention is as follows. The flow directions as shown in Fig. 3 for normal B_t cases are assumed positive. Opposite directions for cases with reversed B_t are also assumed positive. For example, for the interface 3 all flows in Table 1 are positive. This means that in normal B_t cases flow directions as from the outer to inner divertor, and in reversed B_t cases they are from the inner to outer divertor. Any flow through an interface which violates this convention is assumed negative and shown in the table with the minus sign.

Interface→ ↓n_s (E19m^{-3})		1	2	3	4	5
0.7	N.Bt	4.44E21	8.74E21	9.26E21	2.62E21	3.42E21
	R.Bt	1.74E21	1.90E21	1.00E22	6.55E20	2.15E21
0.9	N.Bt	2.70E21	1.49E22	1.39E22	5.12E21	1.90E21
	R.Bt	-6.93E20	6.50E21	9.43E21	6.20E21	8.84E19
1.0	N.Bt	6.54E20	1.37E22	1.58E22	1.03E22	2.26E20
	R.Bt	-1.09E21	7.98E21	9.51E21	9.46E21	-2.21E20
1.4	N.Bt	4.28E21	1.11E22	1.30E22	1.94E22	2.95E21
	R.Bt	6.74E21	6.74E21	6.67E21	6.04E21	-7.09E21

Table 1. Total ion drift flows through the interfaces 1-5. 'N.Bt' refers to normal B_t cases, and 'R.Bt' – to reversed B_t cases. See text for other details.

From Table 1 it follows that not for all cases is the drift flow situation as simple as in Fig. 3. In particular, poloidal drift flows at the entrances to the divertors may change sign. The common feature of almost all cases is that (mostly radial) drift flows in the PFR (through divertor 'legs', interfaces 2–4) are by factor ~ 5 larger than (mostly poloidal) drift flows at entrances to divertors, through interfaces 1 and 5. Drift flows across interface 3 therefore typically create a positive particle source in the inner divertor, and negative in the outer divertor, in the normal B_t configuration, while doing the opposite in the reversed B_t configuration. This is consistent with target density asymmetries seen both in codes and in experiment. It can also be seen from the table that drift flows through interfaces 2-4 are always positive, and the relative magnitude of (radial) drift flows through interfaces 2 and 4 increases as the density is raised, leading to increasing recycling and lower T_e at the targets (see below).

Estimates show that ∇B drift flows in these cases are substantially below E×B flows, so, to the first approximation, one may consider Fig. 3 and Table 1 as approximately representing E×B drift circulation. However, more detailed analysis is desirable of the E×B drift flows alone and the particle sources that they create in the divertor. The aim of calculations based on the EDGE2D-EIRENE output (postprocessing) in the next section is to separate E×B drifts, split them into poloidal and toroidal components, establish the role of each component in the divertor particle balance locally, for each magnetic flux tube, and relate this to plasma parameters profiles at divertor targets.

4. Calculations of E×B drift flows and related particle sources in the divertors

EDGE2D-EIRENE does not have a standard output that allows one to analyse drift flux contributions separately. A fairly easy postprocessing of the code output is however possible that allows one to separate poloidal and radial E×B drift components without having to work through metric coefficients of the non-orthogonal grid and interpolations of cell centre parameters onto cell faces of the grid, and possible errors associated with this. Indeed, plasma electric potential, plasma density and all other parameters necessary to analyze E×B drift fluxes are calculated at cell centres of the EDGE2D-EIRENE grid. It is possible to construct a 'secondary grid' by connecting cell centres along the poloidal direction which corresponds to a number of flux tubes, as shown in Fig. 4. By knowing profiles of plasma density, electric potential and other parameters along boundaries of this grid, which are also elongated in the poloidal direction, one can easily calculate the total radial E×B flow across each tube. By subtracting the two radial flows at the boundaries of each tube, one can then evaluate a particle source due to the divergence of radial E×B drift fluxes in each tube. The grid shown in Fig. 4 consists of 17 tubes for each, inner and outer, divertor, bounded by 18 lines (or surfaces, in 3D). Poloidally, each tube has 20 points (primary EDGE2D-EIRENE cell centres), right up to the cells surrounding the X-point.

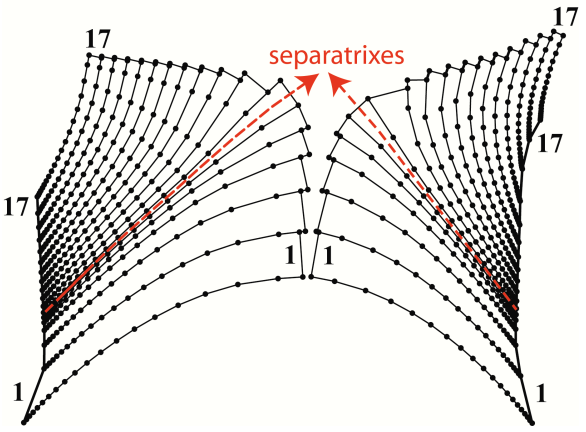

Fig. 4. 'Secondary grid', consisting of flux tubes drawn through centres of the primary grid cells. See text for details.

To calculate poloidal E×B flows into/out of each tube, some end points were eliminated and replaced with interpolated points, with correspondingly interpolated parameters, so that upstream boundaries of the tubes were orthogonal to the poloidal magnetic field. Note that there is an asymmetry between the calculations of radial and poloidal E×B flows: radial flows are calculated as a sum of fluxes through all segments (or surfaces, in 3D), whereas poloidal flows are calculated only through one segment bounding the tubes upstream. The difference between the flows from the three sides of each tube gives a particle source due to the E×B drift which can be compared with changes in ion fluxes at the target surface. In the calculations below, the toroidal surface area factor ($2\pi R$) was taken into account, for easy comparison with flows in Table 1.

The tubes shown do not cover the entire divertor but only the PFR and 12 poloidal rings in the CFR, out of total 20. For rings closer to the wall, drift contributions are typically negligible owing to much smaller electric fields there. Tubes are numbered from 17 to 1, top to bottom along the left divertor (vertical) target plate, and then from 1 to 17 along the right (vertical) target plate.

4.1 Low density cases: separatrix density $n_s=0.7\times10^{19}m^{-3}$

Target parameters for these cases are shown in Fig. 5 in red (solid) for the normal B_t case, in blue (dashed) for the reversed B_t case. As pointed out above, the ion target flow (F_{tar}) gives

the total ion flow to the target bounding each tube, including the surface area factor $2\pi R$. The OMP separatrix T_e for these cases is ≈ 70 eV, hence, owing to the much lower target T_e, recycling in the divertor can be considered at least medium to high, with the exception of the inner target in the normal B_t case with a much higher recycling. Fig. 5 shows typical trends with target asymmetries: in normal B_t cases n_e is larger, and T_e is lower at the inner target, and parameters are much more symmetric in reversed B_t cases. This is also, with rare exceptions, typically observed in experiments.

Diagrams in Fig. 6 show sources due to radial and poloidal E×B flows in each tube, separately, and their sum. Averaged over the whole inner and outer divertors, drifts create a particle source in the inner divertor, and a particle sink in the outer divertor, for normal B_t, with the opposite for reversed B_t cases. Separate calculations of drift particle balances in the CFR and PRF are not trivial, since tubes 6 include the separatrix position, hence, the balance in these tubes partly contributes to the CFR and partly to the PFR. For approximate estimates of particle balances over macrozones, we will attribute half of the balance for tubes 6 balance to the CFR and half to PRF. Clearly, for these low density cases sources in tubes 6 are the largest, which can be attributed to a large poloidal E×B flow in the PFR, in agreement with experimental measurements of Boedo *et al*. [18]. With half of the sources for tubes 6 sources attributed equally to CFR and PFR, it is found that E×B drift adds particles to the inner divertor and removes them from the outer divertor in normal B_t, and has the opposite effect in reversed B_t cases. In the CFR, outside of the separatrix tube, it is the radial E×B drift that is the primary cause of consistency with experiment, and its effect competes with the effect of the poloidal E×B drift. In the PFR, the effect of the poloidal E×B drift dominates, but there it is the primary cause of consistency with experiment.

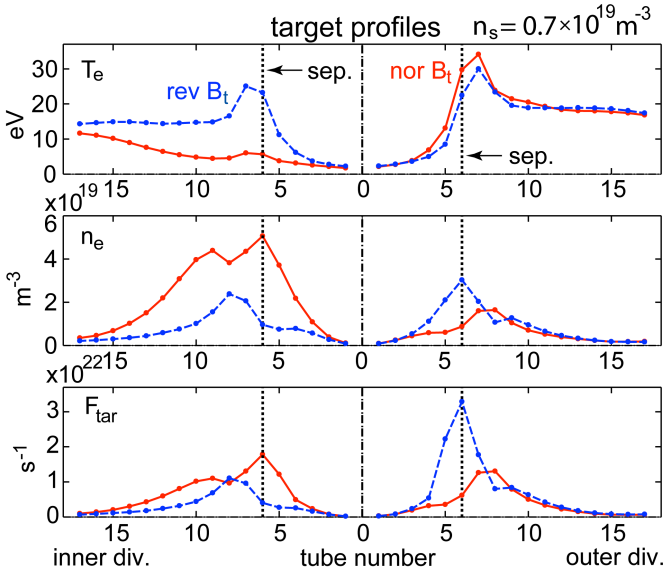

Fig. 5. Target electron temperature, density and ion flux for low density cases with normal and reversed B_t cases with $n_s=0.7\times10^{19} m^{-3}$. Tubes 6 on each, inner and outer divertor side, embrace separatrixes.

For divertor and target parameters, it is probably the average sources and sinks in divertors, rather than local contributions, that matter, owing to the fairly high cross-field neutral propagation. For example, if drifts add particles to one divertor, one can expect larger plasma fluxes to the target in this divertor, larger neutral circulation, and as a result lower T_e. Anomalous diffusion and neutrals mobility should smooth out local drift contributions and shift the overall divertor conditions towards higher or lower recycling.

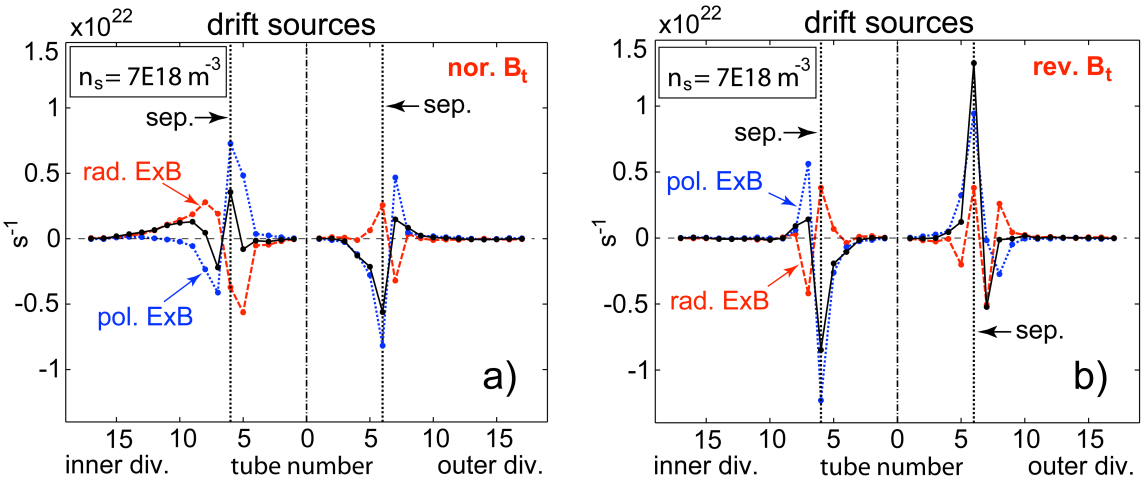

Fig. 6. Particle sources due to radial (red solid lines) and poloidal (blue dotted lines) E×B drifts, and the sum of the two drifts (black solid lines), for low density cases with normal (left diagram) and reversed (right diagram) B_t cases with $n_s=0.7\times10^{19}m^{-3}$.

4.2 Medium density cases: separatrix density $n_s=0.9\times10^{19}m^{-3}$

In these cases, due to higher recycling, maxima of T_e at the inner target are reached outside of the view shown in Fig. 7 (to be visible it would require a ring further radially out, in the far SOL, where particle flux to the target becomes negligible). At the outer target, the T_e maxima are observed at positions of low target particle fluxes. The radially decaying T_e slope at positions closer to the wall is not seen here due to incomplete coverage of the divertor volume in these calculations. (This result, however, is only valid for this particular JET case and geometry).

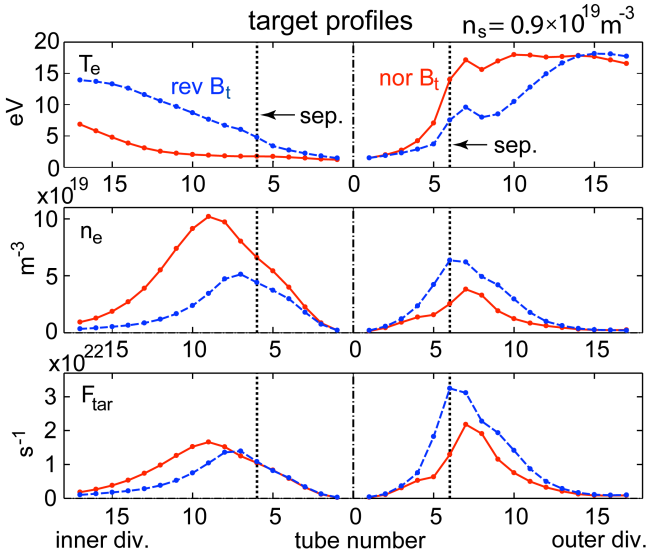

Fig. 7. The same parameters as shown in Fig. 6, but for $n_s=0.9\times10^{19}m^{-3}$.

Sources due to radial and poloidal E×B flows in tubes are shown in Fig. 8. These drifts create sources and sinks in both inner and outer divertor in agreement with density asymmetries seen in the code output. Some oscillations of the curves around pos. 7-8 are probably related to non-monotonic features in outer target T_e profiles. In the CFR, radial drift sources are larger than poloidal, while in the PFR the opposite is true. In either case, both radial E×B drift in the CFR and poloidal E×B drift in the PFR cause density asymmetries consistent with those seen in experiments and codes.

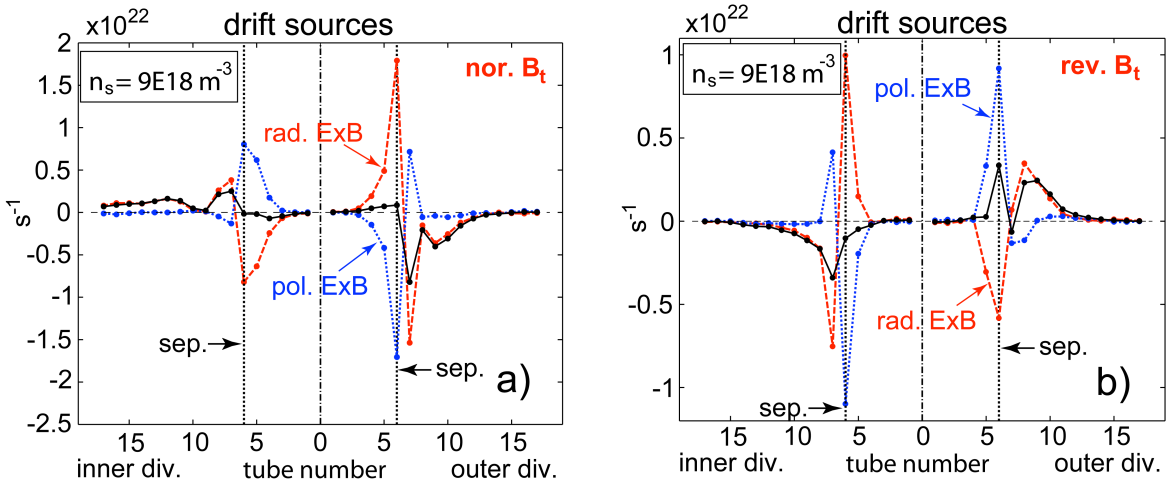

Fig. 8. The same parameters as shown in Fig. 7, but for n_s=0.9×10^{19}m^{-3}.

4.3 High density cases: separatrix density n_s=1.0×10^{19}m^{-3}

In these cases there is almost no indication of even local T_e maxima on the outer target at positions near the maxima of the ion target flux, due to the particular JET divertor geometry and closed divertor configuration. The results are similar to those in the previous case, see Figs. 9 and 10.

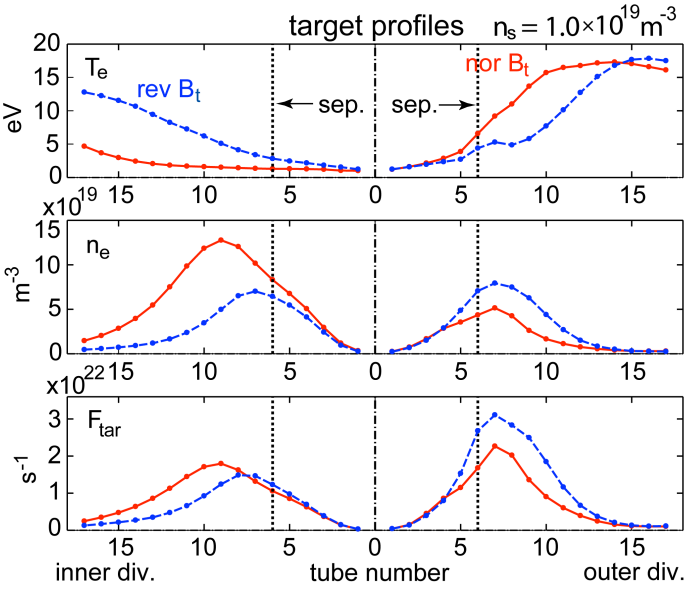

Fig. 9. The same parameters as shown in Fig. 5, but for n_s= 1.0×10^{19}m^{-3}.

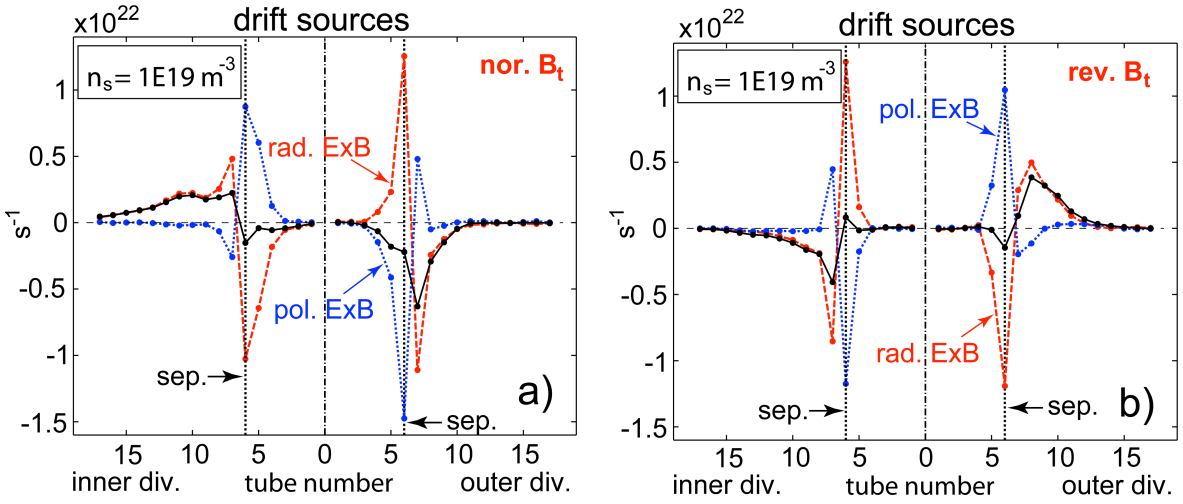

Fig. 10. The same parameters as shown in Fig. 6, but for n_s=1.0×10^{19}m^{-3}.

4.3 Very high density cases: separatrix density n_s=1.4×10^{19}m^{-3}

The tendencies in Figs. 11 and 12 are less clear than at lower densities, but, despite non-monotonic features in profiles of Fig. 12, differences in the sources caused by the B_t reversal are unambiguous.

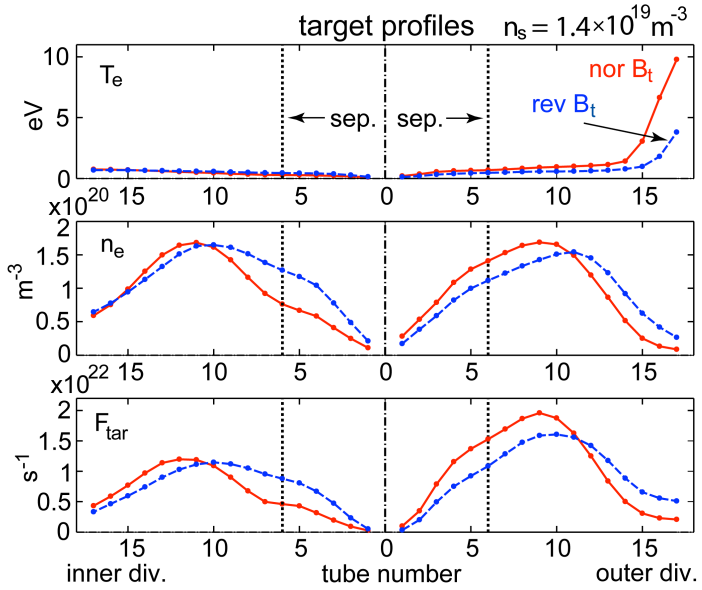

Fig. 11. The same parameters as sho
in Fig. 5, but for n_s=1.4×10^{19}m^{-3}.

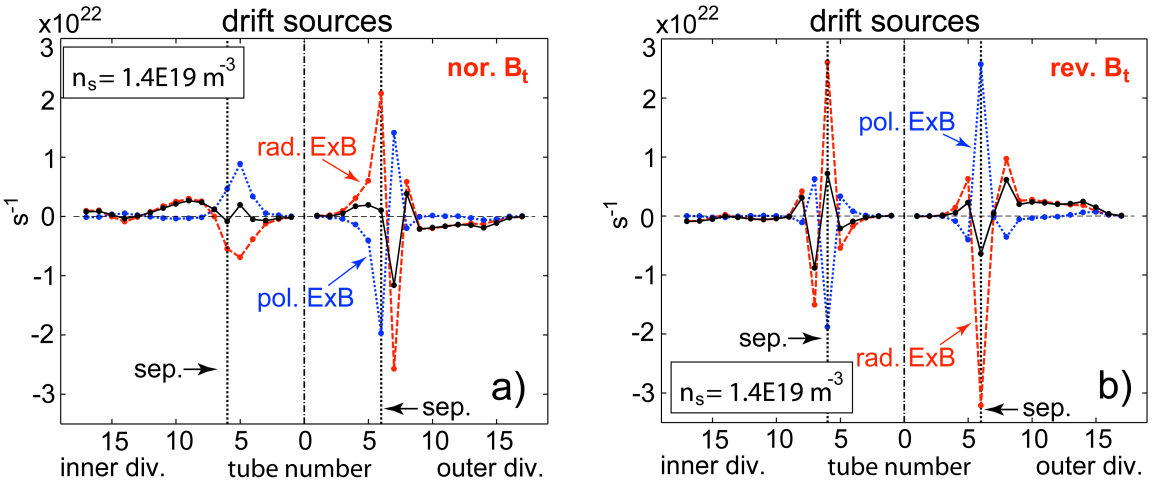

Fig. 12. The same parameters as shown in Fig. 6, but for n_s=1.4×10^{19}m^{-3}.

5. E×B drift flows between macrozones

Here, we present results of our calculations of E×B drift flows through macrozone interfaces. They can be compared with the EDGE2D-EIRENE output for all drift flows combined shown in Table 1. Since boundaries of the 'secondary grid' (flux tubes) don't exactly coincide with the macrozone boundaries, some processing of the E×B drift flow values are necessary:

• to compare with drift flows through interfaces 1 and 5, poloidal E×B flows at tubes 7 to 17, plus ½ of the poloidal E×B flow at tube 6 ('pos. 6', embracing the separatrix), are summed up,

• to compare with drift flows through interfaces 2 and 4, radial E×B flows through (poloidal) boundaries of tubes 6 are averaged,

• to compare with drift flows through interface 3, poloidal E×B flows for tubes 1–5, plus ½ of the flows for tubes 6, are summed up. In addition, these results were averaged between inner and outer divertors. The differences between these flows at different divertors however are not significant, only about 10%. The results are assembled in Table 2.

Interface→ ↓n_s (E19m^{-3})		1	2	3	4	5
0.7	N.Bt	3.34E21	8.78E21	8.83E21	2.03E21	1.69E21
	R.Bt	9.53E19	2.52E21	9.39E21	6.69E20	1.06E21
0.9	N.Bt	1.46E21	1.50E22	1.21E22	4.70E21	-4.94E20
	R.Bt	-2.28E21	6.73E21	7.94E21	6.05E21	-2.99E21
1.0	N.Bt	-5.32E20	1.46E22	1.26E22	9.65E21	-2.87E21
	R.Bt	-2.67E21	8.13E21	8.04E21	9.21E21	-3.35E21
1.4	N.Bt	-2.93E20	1.57E22	1.56E22	2.08E22	8.91E20
	R.Bt	-5.02E21	5.57E21	6.58E21	6.34E21	-9.37E21

Table 2. Calculated ion E×B *drift flows through interfaces 1-5. 'N.Bt' refers to normal B_t cases, and 'R.Bt' – to reversed B_t cases. See text for details.*

One can see that poloidal E×B flows through interfaces 1 and 5, that is, at the entrances to divertors from the main SOL differs strongly with those in Table 1. The large difference between these flows in the two tables is mainly attributed to contributions from the tube 6 (embracing the separatrix), which has the highest flows, and which combines flows in the PFR and CFR. Since flows through interfaces 1 and 5 are smaller than through other interfaces, the error associated with an (implicit) assumption that flows for each tube 6 (embracing the separatrix) should be equally divided between the CFR and PFR, can be large, possibly resulting in the change of the sign. At the same time, already from Table 1 one can see that drift flows through interfaces 1 and 5 show large variations from case to case, often having opposite signs to what one would expect from simple considerations. The most important feature of the calculations made here is that large calculated flows through boundaries close to all other interfaces (2-4) for all other cases are positive, as in Table 1, that is, they have directions expected from the electric potential distribution. Calculated flows through these boundaries correlate very well with the drift flows through macrozone interfaces given in Table 1. This also points to the secondary role played by the ∇B drift in the macrozone balances.

6. Conclusions

Present 2D edge fluid codes with drifts included predict the influence of B_t reversal on divertor and target asymmetries that is in qualitative agreement with experimental observations. Despite this, *understanding* of drift effects was hitherto still missing, with different analytical theories pointing to different drifts or their components as being responsible for the observed asymmetries. Still lacking was the detailed analysis of the code results required to extract information that can shed light on *why* the codes correctly predict trends in divertor and target asymmetries. Qualitative understanding of drift effects is important, since it increases confidence that the most important drift motions and their implementation, including formulation of boundary conditions at the targets, are correctly included in the codes, and that there are no mechanisms of primary importance that are missing in the codes.

In this paper, detailed analysis of convective fluxes caused by E×B drifts in a realistic JET configuration, based on a series of EDGE2D-EIRENE runs, is carried out. The particle fluxes and associated particle sources are calculated separately for poloidal and radial components of the E×B drift. Changes in target asymmetries related to toroidal field reversal are shown to originate from non-divergence-free circulation of E×B fluxes in the divertor. In normal B_t configurations, in the common flux region (CFR) of the divertor ('SOL-divertor') radial divergence of the radial E×B drift flux creates particle sources in the inner divertor, and particle sinks in the outer divertor. The situation is reversed in reversed B_t configurations. In each of the inner and outer divertors, the divergence of radial E×B fluxes is numerically larger than that of poloidal E×B fluxes, with the two divergencies having opposite signs. These results highlight the crucial role of the radial E×B drift in influencing divertor and target asymmetries. They also solve a long standing 'paradox' in understanding the effect of the B_t reversal on divertor and target asymmetries: 'How can it be that the asymmetries observed both in the 2D fluid codes and experiments are opposite to those expected from what has always been regarded as the most clear-cut drift-related mechanism in the SOL, namely, the plasma density redistribution between the two divertors caused by poloidal E×B

drift?' In the private flux region (PFR), where the number of charged particles is less than in the CFR, poloidal E×B drift is dominant, but there its direction is consistent with experimentally measured target asymmetries. Hence, both components of the E×B drift work together to produce target asymmetries observed in experiments, with the leading role played by radial E×B drift in the CFR.

It is also demonstrated (in Appendix A) that statements made in refs. [14-16] about poloidal E×B drift in the SOL and divertor purporting to explain divertor and target asymmetries are unjustified. They follow from erroneous conclusions that poloidal E×B drift reduces plasma density at the target towards which it is directed and increases it at the opposite target.

7. Acknowledgment
This work has been carried out within the framework of the EUROfusion Consortium and has received funding from the European Union's Horizon 2020 research and innovation programme under grant agreement number 633053. The views and opinions expressed herein do not necessarily reflect those of the European Commission.

Appendix A

In this appendix we consider statements made in three recent papers by Rozhansky *et al.* in Refs. [14-16] that poloidal E×B drift reduces plasma density at the target towards which it is directed and increases it at the opposite target. Justifications for these statements are contained in Ref. [14]. Here we consider arguments presented by the authors of this paper in support of their claim. In this appendix by 'authors' we will always understand the authors of Ref. [14], and inverted double quote characters will be used only for citations (in Italics) from this reference.

From the Introduction section of Ref. [14], referring to the poloidal E×B drift, one reads: "*A larger plasma density is observed at the divertor where the E×B drift is directed away from the plate, while the plate where the E×B drift is directed towards the plate has a low density*". This is not only the summary of experimental observations and SOLPS code results, but also a reflection of the authors' perception of causality between the poloidal E×B drift and target asymmetries. In the Conclusion section of Ref. [14], referring to the role of this drift, the authors write: "*The drifts directed away from the plate make the divertor denser and colder, while the drifts towards the plate lead to a decrease in density and increase in temperature*".

To back their claim the authors proposed a simple 1D model consisting of the parallel momentum balance equation with the inclusion of poloidal E×B drift and target boundary conditions with the inclusion of this drift, in Section 4 (Discussion) of Ref. [14]. Coordinate x corresponds to the poloidal direction, and the plasma is contained between the two, left and right, targets (referred to as 'plates' in Section 4 of [14]). The boundary conditions stipulate that parallel ion velocity at the target should react to the poloidal E×B drift towards/away from the target in such a way so as to make the total poloidal ion velocity equal to Θc_s, where $\Theta = B_{pol} / B$ is the ratio of poloidal to total magnetic field and c_s is ion sound speed.

We repeat here the authors' momentum balance equation (Eq. (3) of [14]):

$$m_i \frac{\partial}{\partial x} n V_x V_{||} = -b_x \frac{\partial p}{\partial x}, \qquad \text{(A1)}$$

where n is plasma density, p is plasma pressure, $V_x = b_x V_{||} + V_x^{E\times B}$ ($b_x \equiv \Theta \equiv B_{pol} / B$) is ion poloidal velocity composed of the projection of the ion parallel velocity $V_{||}$ onto the magnetic field line ($b_x V_{||}$) and poloidal E×B drift velocity.

Integrating Eq. (A1) yields ((Eq. 4) of [14]):

$$n V_x (V_x - V_x^{E\times B}) + n b_x^2 c_s^2 = const(x). \qquad \text{(A2)}$$

This equation allows one to obtain the plasma density profile along x direction for a given profile of the ion poloidal velocity V_x.

The authors consider a special case of a very large E×B drift velocity equal to the poloidal projection of the ion sound speed: $V_x^{E\times B} = b_x c_s$, from the left to right target. Given the boundary conditions: $V_x = \pm b_x c_s$ ('+' for the right target and '–' for the left target), this results in $V_{\|} = -2c_s$ (meaning ion parallel velocity from right to left) at the left target and $V_{\|} = 0$ at the right target. Inserting these values into Eq. (A2) directly gives the result that $n_{right} = 3n_{left}$, i.e. that the density at the right target towards which $V_x^{E\times B}$ directed is higher than at the target away from which it is directed. The same result is obtained by inserting these velocities into Eq. (1) of this paper.

As noted, Eq. (A1) is the momentum conservation equation and has to be satisfied independently of the particle conservation equation and of the spatial distribution of ionization sources. Thus the foregoing result that $n_{right} = 3n_{left}$ holds regardless of the spatial distribution of the particle (ion) sources. Nevertheless since the authors have introduced unnecessary complication by discussing the spatial distribution of the ionization sources, we address that in the following.

The authors assume the existence of high recycling zones adjacent to the targets. In Fig. A1, we schematically illustrate the normalized density distribution between the two targets following from the authors' model. Positions A, B, C, D and E refer to the left target, entrance to the high recycling zone at the left target, entrance to the high recycling zone at the right target, position near the right target with the local density maximum, and right target, respectively. The authors obtain that $n_B = 3n_A$ and identify a local maximum at point D with $n_D = 4/3 n_E$, the results we can confirm. They however fail to explicitly give a relation between n_B and n_C, either in terms of equation(s) or by words. Despite that, they made a surprising conclusion, after discussing the factor 4/3 density drop from point D to point E at the right target: "*The density rise from the plate is more modest than at the left divertor and as a result the density at the right divertor and the particle flux to the right plate are smaller*". Setting aside the switch between 'plate' and 'divertor' in this statement, it is illogical, since no relation between n_B, n_C and n_D is explicitly shown in their paper.

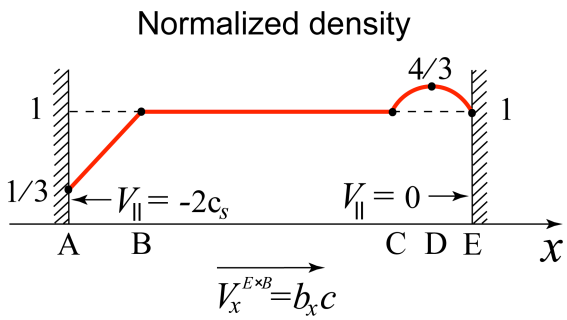

Fig. A1: Schematic density profile normalized to $const/(b_x^2 c_x^2)$, *following from the simplified model* [14].

We discussed the simple model considered in this appendix with the two authors of Ref. [14] (including the first author). They admitted that conclusions about poloidal E×B drift reducing plasma density at the target towards which it is directed and increasing it at the opposite target did not follow from their model. At the same time they argue that their model is to be applied only to the two high recycling zones adjacent to the targets but not to the plasma in between them, and that the constants of integration $const(x)$ to be used near left and right targets may be different. They haven't however provided an alternative relationship between the constants of integration and hence densities at points B and C. We would like to point out, that, judging by their algebra and verbal statements in Ref. [14], the authors assumed 100%

recycling in the 'high recycling zones' and no ionization in the main SOL (no particle sources between points B and C), since they used $V_x = 0$ at point B and "*to the right of the high recycling zone*" up to point C, which makes is inevitable that $n_C = n_B$. In any case, as noted above, the key result that $n_{right} = 3n_{left}$ follows from momentum conservation alone and is unaffected by the spatial distribution of the particle (ionization) sources. It would require the presence of some additional, external force in the region between the targets to alter this relation between the target densities. We therefore conclude that not only the authors' statements about poloidal E×B drift reducing plasma density at the target towards which it is directed and increasing it at the opposite target, are unjustified, but also that, according to their model, exactly the opposite is true, in agreement with predictions of earlier models [3-5].

References

[1] Stangeby P C, in *The Boundary of Magnetic Fusion Devices*, IOP Publishing, Bristol (2000).
[2] Chankin A V, J. Nucl. Mater. **241-243** (1997) 199.
[3] Tendler M and Rozhanksy V, Comments Plasma Phys. Control. Fusion **13** (1990) 191.
[4] Cohen R H and Ryutov D D, Comments Plasma Phys. Control. Fusion **16** (1995) 255.
[5] Stangeby P C and Chankin A V, Nucl. Fusion **36** (1996) 839.
[6] Porter G D, Petrie T W, Rognlien T D, and Rensink M E, Physics of Plasmas 17 (2010) 112501.
[7] Aho-Mantila L, Wischmeier M, Müller H W, et al., Nucl. Fusion **52** (2012) 103006.
[8] Schneider R *et al*., J. Nucl. Mater. **196-198** (1992) 810.
[9] Schneider R, Rozhansky V, Voskoboinikov S, Nucl. Fusion **41** (2001) 387.
[10] Taroni A *et al*., Contrib. Plasma Phys. **32** (1992) 438.
[11] Radford G J *et al*., Contrib. Plasma Phys. **36** (1996) 187.
[12] Rognlien T D *et al*., Contrib. Plasma Phys. **34** (1994) 362.
[13] Rognlien T D and Ryutov D D, Contrib. Plasma Phys. **38** (1998) 152.
[14] Rozhansky V, Molchanov P, Veselova I, et al., Nucl. Fusion **52** (2012) 103017.
[15] Rozhansky V, Molchanov P, Veselova I, et al., J. Nucl. Mater **438** (2013) 297.
[16] Rozhansky V, Contrib. Plasma Phys. **54** (2014) 508.
[17] Aho-Mantila L, Coster D P, Wischmeier M and the ASDEX Upgrade Team, '*On the role of drifts in the divertor power load disstribution in ASDEX Upgrade*', paper O4.120 presented at 41st EPS Conference on Contr. Fusion and Plasma Phys., Berlin, 23-27 June 2014, ECA Vol. **38F** (2014) .
[18] Boedo J A, Schaffer M J, Maingi R, and Lasnier C J, Phys. Plasmas **7** (2000) 1075.
[19] Chankin A V and Stangeby P C, '*Global Circulation of Drift Flows in the SOL and Divertor and its Impact on Divertor Asymmetries*', paper O-4.1C presented at 30th EPS Conference on Contr. Fusion and Plasma Phys., St. Petersburg, 7-11 July 2003, ECA Vol. **27A** (2003).
[20] Schaffer M J, Bray B D, Boedo J A, et al., Physics of Plasmas **8** (2001) 2118.
[21] Groth M et al., '*Divertor Plasma Conitions and Neutral Dynamics in Horizontal and Vertical Divertor Configurations in JET-ILW Low Confinement Mode Plasmas*', presented at the 21st Conference on Plasma Surface Interactions in Controlled Fusion Devices, 26-30th May 2014, Kanazawa, Japan, paper P1-073.